NOVEMBER 1975 MATT-1165

Conf-750723--19

COUNTERSTREAMING-ION TOKAMAK NEUTRON SOURCE FOR LARGE-AREA SURFACE RADIATION STUDIES

D. L. JASSBY

PLASMA PHYSICS LABORATORY

PRINCETON UNIVERSITY
PRINCETON, NEW JERSEY

This work was supported by U. S. Energy Research and Development Administration Contract E(11-1)-3073. Reproduction, translation, publication, use and disposal, in whole or in part, by or for the United States Government is permitted.

DISCLAIMER

NOTICE

Printed in the United States of America.

Available from
National Technical Information Service
U. S. Department of Commerce
5285 Port Royal Road
Springfield, Virginia 22151
Price: Printed Copy $ *; Microfiche $1.45

*Pages	NTIS Selling Price
1-50	$ 4.00
51-150	5.45
151-325	7.60
326-500	10.60
501-1000	13.60

COUNTERSTREAMING-ION TOKAMAK NEUTRON SOURCE FOR LARGE-AREA SURFACE RADIATION STUDIES *

D. L. Jassby

Plasma Physics Laboratory, Princeton University,
Princeton, New Jersey 08540

ABSTRACT

A tokamak neutron source that produces a neutron flux ~ 10^{13} n/cm^2/s over a wall test-area of 30 m^2 is designed using near state-of-the-art tokamak and neutral-beam injection technologies. To maximize fusion reactivity, D and T plasma ions are grouped in two distinct quasi-thermal velocity distributions, oppositely displaced in velocity along the magnetic axis. Such counterstreaming distributions can be set up by tangential injection of all plasma ions by oppositely directed D and T neutral beams, by facilitating removal of completely decelerated ions, and by minimizing plasma recycling. Fusion energy is produced principally by head-on collisions between D and T ions in the counterstreaming distributions. For injection energies of 40-60 keV, and typical tokamak parameters, the fusion power density can be ~ 1 W/cm^3, with Q ~ 1 attainable for T_e = 3.4 keV and electron energy confinement parameter $n_e \tau_E \simeq 2 \times 10^{12}$ cm^{-3}s. All plasma fueling is carried out by the injected beams, and when a significant fraction of the electron population is trapped, the plasma current can be maintained by the beams.

The parameters of this tokamak neutron source are the following: plasma radius = 55 cm, R/a = 5.1, vertical elongation = 1.30, B_t = 40 kG, W_{beam} = 60 keV, P_{beam} = 21 MW, $\bar{n}_e = 4 \times 10^{13}$ cm^{-3}, $\bar{T}_e$ = 4 keV, I_p = 1.4 MA, $n_e \tau_E = 2 \times 10^{12}$ cm^{-3}s, duty factor > 68%. The 14-Mev neutron production is 9.6×10^{18} n/s, with a peak flux at the wall of 8.4×10^{12} n/cm^2/s, or an annual fluence of 10^{20} n/cm^2 with 38% plant factor. The tritium throughput is 12 g/hr, with a fractional burn-up per pass of 1.1%. The 40-kG toroidal field is provided by a hybrid magnet composed of copper coils and NbTi coils. The maximum field at the NbTi is 65-70 kG. The test sample volume is a 20-cm thick semi-toroidal shell on the outer region of the torus, and the useful test area is about 30 m^2. The electrical power consumption of the entire facility is 97 MW, and the total estimated cost, including buildings, remote handling, and tritium handling, is $139M.

* Presented at International Conference on Radiation Test Facilities for the CTR Surface and Materials Program, July 15-18, 1975, Argonne National Laboratory, Argonne, Illinois, USA.

1. INTRODUCTION

The first walls of toroidal fusion reactors must withstand quasi-continuous 14-MeV neutron fluxes in the range $3 \times 10^{13} - 2 \times 10^{14}$ n/cm^2/s. The durability of structural materials to such intense fluxes over periods of many years can be estimated only poorly, and many proposals have been made for the construction of test facilities to study radiation damage in a variety of materials [1]. While information on bulk radiation damage (e.g., voids, creep, swelling) is required ultimately, surface-radiation damage information (e.g., sputtering, blistering) is perhaps most urgent for near-term fusion reactor applications. Significant surface damage is expected to arise in many materials subjected to 14-MeV neutron fluence in the range 10^{19}-10^{20} n/cm^2. The requirements of a surface radiation effects facility are [2]:

(1) Production of a fluence of 10^{20} n/cm^2 in a reasonable time, such as 6-12 months.

(2) Ability to accommodate simultaneously a large number of radiation experiments.

(3) Ease of access and instrumentation of the test volume.

(4) Relevant neutron spectrum.

(5) Possibly the investigation of synergistic effects, which might result from the simultaneous bombardment by energetic particles, photons, and neutrons.

(6) Cost-effectiveness, which can perhaps be measured by neutrons/sec/M$ capital cost, or by neutrons/sec/MW, which reflects operating cost.

If the ultimate objective of such radiation damage studies is to aid in the development of tokamak power reactors (or other quasi-stationary toroidal fusion reactors), then it appears that one should consider tokamaks themselves as possible radiation facilities. Obvious advantages of a tokamak facility are that the neutron spectrum and "synergism" are most appropriate, and that development expenditures are made in the field of tokamak technologies — rather than for other equally difficult technologies that may lead to intense 14-MeV neutron production, but cannot be used in tokamak power reactors.

A near-term radiation effects facility must utilize essentially state-of-the-art technology. This paper considers the design of a beam-injected tokamak neutron source with a plasma size characteristic of machines presently coming into operation (e.g., T-10, PLT), and with neutral beam injection voltages in the range 40-60 keV, where high-power beams have already been produced. The machine described herein furnishes a time-averaged neutron flux in the range 5×10^{12} -10^{13} n/cm^2/s over a test area of some 30 m^2, and meets all the requirements listed above. This device appears to be the most cost-effective radiation source for surface effects studies, and its construction and operation would enable considerable development of tokamak reactor technologies.

In order to attain large neutron fluxes with modest plasma size and small injected-beam voltage, the tokamak plasma-beams system must be operated in the counterstreaming-ion mode [3,4], whereby D and T neutral beams are injected in opposite toroidal directions, and particle recycling is prevented in order to minimize the cold-ion population. The physics of counterstreaming-ion tokamak (CIT) plasmas is reviewed in Sect. 2, while CIT reactor aspects are discussed in Sect. 3. Section 4 presents the basic parameters for the reference design. Section 5 discusses engineering aspects, including the cost of the facility and the various technological developments required.

2. PHYSICS OF CIT OPERATION

Consider a toroidal plasma in which the D and T ions are grouped in two distinct, quasi-thermal velocity distributions, oppositely displaced in velocity along the magnetic axis, as shown in Fig. 1. The relative displacement velocity v_r is near the optimum value for generating fusion power, which occurs principally by nearly head-on collisions between D and T ions of the counterstreaming distributions. Such distributions can be set up by introducing all ions by means of neutral beams injected parallel and anti-parallel to the toroidal magnetic field. The energetic ions slow down by Coulomb drag on the plasma electrons, and if completely decelerated ions are removed from the plasma in a time that is short compared with the fast-ion slowing-down time, virtually all plasma ions will be found in the toroidally directed "beams". We refer to this system of space-charge neutralized ion distributions as a counterstreaming-ion toroidal plasma, or CIT. Evidently, head-on nuclear collisions permit beam injection energies to be 3 or 4 times smaller than in beam-target systems, for the same fusion reactivity.

2.1 Ion Velocity Distributions

A target plasma, which can be a low-temperature tokamak plasma, is required to initiate CIT operation. Once beam injection has begun, magnetic divertor coils are energized, so that recycling of outwardly diffusing ions is minimized: The inward flow rate of cold neutrals and ions from the wall region must be kept small compared with the rate of particle injection by the beams. After injection for several slowing-down times, T_e reaches an equilibrium value, and the ion population is dominated by energetic ions. In the following, we consider only steady-state CIT operation.

Energetic ions are assumed to be confined until they decelerate to an energy $W \sim 2T_e$. Ions with energy $W < 2T_e$ are assumed to be lost at a rate $\tau^{-1} \sim \tau_E^{-1}$, where τ_E is the electron energy confinement time. Fokker-Planck analysis [3,5] has shown that Coulomb collisions among ions of the same beams cause significant energy diffusion during the slowing-down process, while interaction between ions in opposite beams tends to produce angular scattering. As a result of these processes, the ions in each beam tend to form a "thermal" distribution, with a mean velocity in the laboratory frame somewhat less than the injection velocity, v_o. Reference [4] describes a simple physical model that provides ion distribution functions which can be used to predict CIT properties (e.g., $n_e\tau_E$ vs T_e, Q vs T_e) that are in good agreement with the results of Fokker-Planck calculations. In this model, the ions in each beam form a displaced Maxwellian of temperature T_b:

$$f(\vec{v}) = \left(\frac{M}{2\pi T_b}\right)^{3/2} \exp\left[-\frac{M}{2T_b}(\vec{v} - v_p\hat{\phi})^2\right] \quad (1)$$

Here $\hat{\phi}$ is the unit vector along the magnetic axis, and $v_p = (2W_s/M)^{1/2}$, where W_s is the average energy of a test ion that slows down to an energy $2T_e$ by Coulomb drag on plasma electrons, but has no interaction with other ions. The parameter T_b is found by postulating an equipartition of energy between the directed ion motion and the plasma thermal motion:

$$\frac{1}{2} M v_p^2 = 3/2\ T_e + 3/2\ T_b \quad (2)$$

Distribution functions for D° and T° injected at W_o = 60 keV and T_e = 4 keV are shown in Figs. 1 and 2. For this example, $v_p = 1.46 \times 10^8$ cm/s and T_b = 10.5 keV. For practical values of W_o, T_e, and T_b, the CIT plasma should be stable to electrostatic and electromagnetic velocity-space modes [3,6].

2.2 Power Balance and Energy Confinement

The electron temperature is maintained almost entirely by power flow from the fast ions. (Ohmic heating provides $\lesssim$ 10% of the total power input.) T_e is found from the steady-state power balance relation

$$\frac{3}{2}\frac{n_e T_e}{\tau_E} = \frac{C n_e \ell n \Lambda_e}{T_e^{3/2}} \sum_{D,T} \frac{n_i (\bar{W}_i - 3/2 T_e)}{A_i} \quad (3)$$

where $C = 1.06 \times 10^{-13}$ (T_e, W in keV), n_i is the density, A_i the atomic mass, and W_i the average ion energy in each beam:

$$\bar{W} = \frac{1}{2} M v_p^2 + 3/2\ T_b \quad (4)$$

If $Z = 1$, then $n_e = n_D + n_T$. In this paper, we consider only cases where $n_D = n_T$ and $W_{oD} = W_{oT}$. Given T_e and W_o, $\bar{W}$ is readily found, and Eq. (3) gives the unique value of $n_e\tau_E$. In practice, T_e and n_e are determined by τ_E and the energetic-ion source strength S. Therefore, we plot in Fig. 3 the T_e that is produced for a given $n_e\tau_E$ and W_o. Evidently, very large T_e can be attained with relatively modest $n\tau$ values.

The ion source strength is

$$S_i = \frac{n_i}{\tau_{hi}} \quad (5)$$

where τ_{hi} is the ion lifetime. Defining $\tau_h^{-1} = (\tau_{hD}^{-1} + \tau_{hT}^{-1})/2$, τ_h/τ_E is given by

$$\frac{3}{2}\frac{n_e T_e}{\tau_E} = \frac{n_e (W_o - \gamma T_e)}{\tau_h} \quad (6)$$

where $\gamma T_e \sim 3/2\ T_e$ is the average energy of the ions leaving the plasma. For most conditions ($W_o \gg T_e$), the ion lifetime must be many times τ_E. This requirement seems compatible with observations on beam-injected tokamak

plasmas [7], where in the absence of charge-exchange losses, the energetic ions remain in the plasma for their slowing-down time $\gtrsim$ 10 ms, while τ_E is in the range 2-5 ms.

2.3 Neutral Beam Trapping

Neutrals injected into the steady-state CIT plasma are trapped by the energetic ions in the counterstreaming distributions, and by electron ionization. The relative collision energy U between a tangentially injected deuterium atom (D°) and the D^+ ions is very small (e.g., U $\simeq$ 7 keV for the conditions of Fig. 1), while U for collisions between the D° and the T^+ ions is very large (U $\simeq$ 140 keV for the same case). Approximately half the D° are trapped by charge exchange with D^+, and the other half by impact ionization on T^+, and by electron ionization. Calculation of the neutral penetration length λ_t is discussed in [4]. The results are shown in Fig. 4(a) for $n_e = 5 \times 10^{13}$ cm^{-3} and $T_e = 4.0$ keV. λ_t is inversely proportional to n_e, but very weakly dependent on T_e.

Also shown in Fig. 4(a) is the probability of the injected neutral being trapped by charge exchange. The average energy of the secondary neutral is in the range 0.6 - 0.9 $\bar{W}$, depending on W_{OD} and T_e. This neutral will be travelling nearly parallel to the magnetic axis, and will undergo charge-exchange or ionization before escaping. Successive generations of neutrals are formed in this way, until finally ionization occurs, or the neutral escapes. Reference [4] shows that for aspect ratio A = 5.0, plasma radius $a_p = \lambda_t$, $T_e = 4$ keV, and $W_{OD} = 60$ keV, the 4th or 5th generation neutral is lost, so that the fraction of the injected energy lost by charge exchange is 10% or less. Ideally, neutrals enter the plasma only by beam injection (recycling is not permitted), so that the trapping process accounts completely for charge-exchange loss.

2.4 Particle Recycling, Removal, and Impurities

In order to maintain the ideal velocity distributions shown in Figs. 1 and 2, two conditions must be met:

(1) The rate of recycling of cold ions and neutrals must be small compared with the rate of particle input by the neutral beams. This condition can probably be met with the use of a poloidal magnetic divertor that exhausts from the torus those ions diffusing out of the reacting plasma. Even in tokamaks without divertors, it has been found that particle recycling can be greatly reduced by special measures: In the Alcator device, where special discharge-cleaning techniques are employed, the density drops continuously in time unless puffs of gas are injected into the plasma [8]. In the ATC device, the same result is obtained by titanium gettering of the wall [9].

(2) Completely decelerated ions (those with $W < 2T_e$) must be removed from the plasma in a time τ that is short compared with their slowing-down time; i.e., $\tau \ll \tau_h$. There are several processes that would be effective for the rapid removal of decelerated ions:

(i) Instability-Induced Diffusion. Drift-type instabilities cause negligible radial diffusion of energetic ions, because of the short

wave-particle correlation times [10], but they should be effective in enhancing the loss of thermal ions and electrons. Microinstability-induced turbulence causes comparable loss rates of particles and energy, so that if this process is chiefly responsible for the electron energy loss rate τ_E^{-1}, one expects $\tau^{-1} \sim \tau_E^{-1}$.

(ii) Charge-exchange. An appreciable fraction of the charge-exchange losses considered in Sect. 2.3 involve the loss of low-energy ions.

(iii) Toroidal magnetic field ripple. Ripple in the toroidal magnetic field can lead to enhanced diffusion of thermal plasma particles [11]. The ripple can be localized to the outer region of the plasma, so that the only ions affected would be colder ions that have gradually diffused outward during their slowing-down period following injection. In any event, the energetic ions travel nearly parallel to the toroidal field, and cannot be trapped in the ripple field until they have lost most of their energy.

The principal effect of impurity ions in the CIT is to enhance pitch-angle scattering, which undermines the advantage of head-on collisions, and increases the trapping rate of energetic ions. A second deleterious effect is the additional Coulomb drag on energetic ions by the impurity ions and their neutralizing electrons. Preliminary results in [3,5] indicate that for W_o = 60 keV, T_e = 5 keV, and iron impurity, fusion gain Q (Sect. 3.1) is reduced by 33% and 46% for Z_{eff} = 2 and 3, respectively. Impurity radiation losses tend to make up only a small fraction of the total power balance in a highly beam-driven plasma such as the CIT. Impurity reduction of the neutral-beam penetration length [12] is less important than in the TCT case, because impact ionization in the CIT account for only about one-half the trapping rate.

While the impurity population can presumably be minimized by the magnetic divertor (which must be installed to prevent recycling), it is relevant to note that Z_{eff} = 1 plasmas (after correction for electron trapping) have been attained in the Alcator [8] and ATC [9] devices without a divertor — under the conditions noted above.

2.5 Maintenance of Toroidal Current

The counterstreaming-ion distributions have currents associated with them. In Ref. [4], it is shown from momentum-balance equations that when Z_{eff} = 1, the total plasma current is zero unless an external electric field $\vec{E}$ is applied. If the plasma has an impurity population, or if a significant fraction of the electrons are trapped in banana orbits or in toroidal field ripple, then $Z_{eff} > 1$, and a toroidal current can be maintained even when E = 0 [13]. Beam maintenance of the toroidal current is much easier in the CIT case, where essentially all ions are injected via the beams, than in the TCT case, where a low-energy beam of uncertain penetration must be injected to balance the target-ion momentum [14]. Since fueling of the CIT plasma is carried out solely by the injected beams, it appears that virtually steady-state operation is attainable in principle.

3. REACTOR ASPECTS OF CIT OPERATION

3.1 Fusion Power Multiplication and Power Density

The fusion reactivity of the system of counterstreaming D and T ions, using Eq. (1) for the distribution functions, is [4]

$$\langle\sigma v\rangle_c = \frac{\int_o^{v_{max}} dv_{12}\, \sigma(v_{12}) v_{12}^2 \left(e^{C_1 v_{12}} - e^{-C_1 v_{12}}\right) e^{-\mu v_{12}^2/2T_b}}{\int_o^{v_{max}} dv_{12} v_{12} \left(e^{C_1 v_{12}} - e^{-C_1 v_{12}}\right) e^{-\mu v_{12}^2/2T_b}} \qquad (7)$$

Here we have taken $W_{oD} = W_{oT}$, and $v_{max} >> |v_{pD}| + |v_{pT}|$. Also $\mu = M_D M_T/(M_D + M_T)$, $C_1 = (1 + \sqrt{2/3})\, \mu v_{pD}/T_b$, and $\sigma(v_{12})$ is the fusion cross section for D and T nuclei with relative collision velocity v_{12}. Figure 5 shows $\langle\sigma v\rangle_c$ as a function of $v_r = |v_{pD}| + |v_{pT}|$, the relative displacement of the peaks of $f_D(\vec{v})$ and $f_T(\vec{v})$ [Fig. 1]. As $T_b \to 0$, the peak value of $\langle\sigma v\rangle_c$ approaches the maximum value for a beam-target system (1.67×10^{-15} cm^3/s for W = 128 keV). For any T_b, $\langle\sigma v\rangle_c$ can be larger than the maximum reactivity of a thermonuclear plasma, viz. 8.8×10^{-16} cm^3/s at T_i = 60 keV. Thus in the CIT mode, a low-temperature distribution of ions may have a very large fusion reactivity.

In steady-state operation, the fusion power multiplication is $Q = P_f/P_b$, where P_f is the fusion power density and P_b is the injected power density:

$$P_f = n_D n_T \langle\sigma v\rangle_c E_f = \frac{1}{4} n_e^2 \langle\sigma v\rangle_c E_f , \qquad (8)$$

where E_f = 17,600 kev, and $n_D = n_T = \frac{1}{2} n_e$. Defining τ_h as in Eq. (6),

$$P_b = \frac{W_{oD}\, n_D}{\tau_{hD}} + \frac{W_{oT}\, n_T}{\tau_{hT}} = \frac{W_o n_e}{\tau_h} . \qquad (9)$$

Then

$$Q = \frac{1}{6} \langle\sigma v\rangle_c \frac{E_f}{W_o} \frac{n_e \tau_E (W_o - \gamma T_e)}{T_e} \qquad (10)$$

T_e and $n_e\tau_E$ are related by Eq. (3). In practice, T_e and n_e are determined by the τ_E that is characteristic of the plasma, and by the beam source strength, S. Figure 6 shows that for $W_{oD} = W_{oT} = 60$ keV, $Q = 1$ ("break-even") is attained at $n_e\tau_E = 1.4 \times 10^{12}$ cm^{-3}s and $T_e = 3.3$ keV. The required ion confinement time is given by Eq. (6), and for these conditions is $n_i\tau_h = 1.5 \times 10^{13}$ cm^{-3}s. Figure 7 shows the dependence of Q on W_o and T_e. For each T_e, there is a broad maximum in the range $W_o = 40$-60 keV, corresponding to a relative collision energy of 130-200 keV at injection. The maximum pressure p of a tokamak plasma is given by the MHD equilibrium condition on the poloidal beta:

$$\beta_p = \frac{8\pi p}{B_p^2} = \frac{8\pi p\, q^2 A^2}{B_t^2} \leq A \qquad (11)$$

where $A = R/a_p$ is the aspect ratio, and q is the safety factor at the limiter. Then P_f is found from Eqs. (7) and (8), using

$$n_D = n_T = \frac{1}{2} n_e = \frac{\frac{1}{2} p}{T_e + 2/3\, \bar{W}} \qquad (12)$$

Figure 8 shows Q vs P_f for $p = 0.19$ J/cm^3, corresponding to $B_t = 50$ kG, $q = 2.5$, $A = 5.0$, $\beta_p = 3.0$. Each point on a constant-W_o curve corresponds to a particular value of $n_e\tau_E$, and therefore a definite T_e given by Eq. (3). There is a trade-off between P_f and Q, the largest values of P_f being obtained at the smallest $n_e\tau_E$ and T_e. This low-$n_e\tau_E$ region is the most attractive for maximizing neutron production.

3.2 Neutron Production and Wall Loading

Figure 9 shows the 14-MeV neutron production rate from CIT plasmas of circular cross section as a function of a_p and W_o, when $n_e\tau_E$ is such that $T_e = 4.0$ keV (cf. Fig. 3). For a given a_p, the neutron output is proportional to $n_e^2\langle\sigma v\rangle_c$. At small W_o, n_e is determined by the neutral-beam penetration requirement, which we take as $\lambda_t = a_p$. At large W_o, n_e is limited by the allowed plasma pressure, which we take to satisfy $\beta_p = 2/3A$. Therefore, for each a_p there is an optimal W_o that provides maximum neutron output. Evidently, for tokamak plasmas of PLT size ($a_p = 40$-50 cm), and using beam voltages at which high-power neutral beams are now available ($W_o \sim 40$ keV), neutron intensities in the range 10^{18}-10^{19} s^{-1} are attainable.

In the case of a circular plasma with uniform n_e and T_e, and a circular vacuum chamber of radius a_w, the neutron wall loading is

$$WL = 0.40\, P_f \left(\frac{a_p}{a_w}\right) a_p \qquad (13)$$

Figure 10 shows WL vs a_p and W_o, for the same conditions as Fig. 9, and $a_w - a_p = 20$ cm. The wall loading is limited to less than 0.2 MW/m^2 (0.9×10^{13} n/cm^2/s) unless very large plasma radii and beam energies are used. However, the efficiency of neutral-beam injectors (without direct

conversion) decreases drastically for $W_o \gtrsim 80$ keV. Somewhat large WL can be obtained by using a noncircular plasma cross section, or by slightly relaxing the condition $\lambda_t = a_p$, but it appears that WL of the magnitude required to study neutron-induced bulk-radiation effects (~1 MW/m^2) cannot be achieved in a CIT reactor. (A target-plasma reactor has been proposed for this purpose [15].)

3.3 Tritium Burn-Up

An important figure-of-merit is the fractional burn-up of tritium per pass. A large fractional burn-up implies a small tritium throughput per unit neutron production, so that the tritium inventory can be smaller, and the demands on the tritium processing system are reduced. If f_B is the fractional burn-up of tritium (once-through the torus), then

$$\frac{n_T}{\tau_{hT}} f_B E_f = P_f \doteq Q P_b \qquad (14).$$

Using Eq. (9) and $\tau_{hT} = 1.5\ \tau_{hD}$, we have

$$f_B = \frac{Q W_o}{E_f}\left(1 + \frac{\tau_{hT}}{\tau_{hD}}\right) = 2.5\frac{Q W_o}{E_f} \qquad (15)$$

It is evident from the Q-values of Fig. 7 that f_B increases rapidly with T_e, but rather slowly with W_o. At $W_o = 60$ keV, f_B is 0.4% at $T_e = 2$ keV, and 3.9% at $T_e = 12$ keV.

3.4 Effect of a Cold Ion Population

If the particle recycling rate cannot be made insignificant (e.g., if no divertor is provided), or if completely decelerated ions do not rapidly leave the discharge, then a "cold" ion population at a temperature $T_i \approx T_e$ will be present. The reactivity of the total ion population can be seriously reduced, since the relative velocity between the "cold" ions and the energetic ions is well below the optimum value for fusion production. Provided that beam self-collisions continue to dominate during the slowing-down process, an approximate expression for the velocity distribution of each ion species is

$$f(\vec{v}) = \alpha_c \left(\frac{M}{2\pi T_e}\right)^{3/2} \times \exp\left[-\frac{Mv^2}{2T_e}\right] + \left(\frac{M}{2\pi T_b}\right)^{3/2} \times \exp\left[-\frac{1}{2}\frac{M(\vec{v}-\vec{v}_p)^2}{T_b}\right] \qquad (16)$$

where α_c is the ratio of the number of "cold" ions (at temperature T_e) to the number of energetic ions. Figure 11(a) shows the fusion reactivity as a function of α_c, taking into account all possible D-T fusion reactions among

hot and cold components. When $\alpha_c = 1$, $\langle\sigma v\rangle$ is reduced by 50-70%.

On the other hand, the neutron intensity from a given size device need not drastically decrease in the presence of a cold ion population. If α_c increases, the average ion energy decreases, so that the same pressure can support a larger plasma density (cf. Eq. 12), and therefore a larger beam injection rate.

Figure 11(b) shows that for constant p, P_f decreases rather slowly with α_c. While the allowed increase in n_e would in practice be limited by difficulty in beam penetration, it turns out that for $\alpha_c \sim 1$ and $W_o \gtrsim 60$ keV, the reduction in neutron output need be only about one-third.

(Although Q is reduced by at least 50% when $\alpha_c \sim 1$, Q is not as important as sheer neutron production in a radiation test facility. Reference [16] calculates Q-values for a counterstreaming system using a treatment that is appropriate when the cold-ion population is dominant, that is, $\alpha_c \gg 1$.)

4. BASIC PARAMETERS OF THE CIT RADIATION FACILITY

4.1 Choice of Injection Energy

The chief advantage of operating at very low neutral beam energy (30-40 keV) is efficiency of production. For example, overall efficiencies of 60% (busbar-to-beam) have been achieved for D° beams at 40 keV (although present-day beams contain appreciable fractions of D_2° and D_3°). Figure 7 shows that, ideally, maximum Q is attained in the range $W_o \cong 40$-50 keV, when $T_e = 3$-10 keV. Nevertheless, there are several reasons for preferring somewhat larger beam energies:

(1) The attainable neutron intensity increases with W_o (Fig. 9), although the corresponding plasma size must also increase.

(2) If a substantial cold-ion population is present, at larger W_o one can take better advantage of target-plasma reactions. so that neutron flux is not as severely degraded (Fig. 11).

(3) Charge-exchange energy loss (Sect. 2.3) decreases with increasing W_o.

(4) If $Z_{eff} > 1$, angular scattering is reduced at larger W_o.

Satisfactory injector efficiency ($\gtrsim$ 40%) can be attained up to about 80 keV for D° and 120 keV for T°, and to even larger energies if direct conversion of unneutralized ions is utilized. At any rate, given a desired flux level and available magnetic field, the size of the plasma and the optimal W_o are fairly closely determined. In the present design, where a neutron flux $\sim 10^{13}$ n/cm^2/s is desired, the plasma is somewhat elongated, the axial field is 40 kG, and the beam energy is chosen to be 60 keV.

While 90 keV T° beams are produced with the same efficiency and have the same plasma penetration as 60-keV D° beams, the present design specifies 60-keV T°, so that all injectors have identical power supplies. The trapping

profiles of T° and D° beams of equal energy can be made more similar by injecting T° in the direction of the current, so that the T^+ drift surfaces shift inward, while the D^+ drift surfaces shift outward. In practice, the relative energies of the D° and T° beams may be adjusted to produce a specified beam-induced current [13].

4.2 Plasma and Machine Parameters

Long pulses and large duty factor are necessary for obtaining large neutron fluence from a tokamak reactor. While room-temperature copper TF (toroidal field) coils can be designed to produce a steady-state axial field of 30-33 kG, superconducting coils are required for obtaining higher fields, and of course are essential if power consumption must be minimized. Because superconducting TF coils must be protected by approximately 70 cm of shielding, in a small machine an axial magnetic field significantly larger than 30 kG cannot be obtained, if NbTi is the coil material. This situation can be resolved by a hybrid magnet design, whereby some of the shielding volume is taken up by water-cooled copper coils, which then permit a reduction in the maximum field at the NbTi [17]. The copper coils of the hybrid magnet in the present design supply a relatively small field (10 kG on axis), and therefore can be operated steady state.

A schematic layout of the CIT reactor is shown in Fig. 12. The dimensions have been chosen to give the smallest possible device that provides a peak neutron flux ~ 1×10^{13} n/cm^2/s. The major radius of the plasma is determined by the minimum allowed thicknesses of the air-core region, the toroidal field coils, and the shilding required to protect these coils. The core size shown allows a flux swing of 15 volt-sec, which is adequate for driving currents up to 1.5 MA for periods up to at least 30 s. Most of the thermal output of the reacting plasma is removed by a coolant that flows in the shielding region; the remainder of the heat load is removed in the divertor chamber. The total copper-plus-shield thickness of 70 cm adequately protects the copper stabilizer in the superconducting coils, when the uncollided neutron flux $\phi_n \lesssim 10^{13}$ n/cm^2/s. A scrape-off thickness of 20 cm is required for satisfactory operation of a poloidal magnetic divertor [18]. As a result of these considerations, the inner edge of the plasma column is located at 2.25 m.

The present design calls for operation at W_o = 60 keV and T_e = 4.0 keV, so that the ideal Q is slightly larger than unity (Fig. 7). The fusion power density is then given by

$$P_f = 5.16 \times 10^{-4} \left(\frac{B_t}{qA}\right)^4 \beta_p^2 K^4 \qquad (17)$$

where B_t is the field on the magnetic axis (in kG), and K = (plasma circumference) / $2\pi a_p$. The neutron flux requirement is met with B_t = 40 kG, a_p = 55 cm, and a D-shaped plasma cross section with maximum elongation of 1.30, so that K = 1.40. Other plasma parameters are shown in Table I. The inside-D cross section envisioned here is convenient for the implementation of a double-null poloidal divertor [18]. The maximum field at the NbTi is

nominally 65 kG, although leakage field from the copper coils, and contributions from the poloidal field of the plasma current and the vertical equilibrium field, increase the total field strength to 70-75 kG, which is still acceptable. (Without the copper TF coils, the field at the NbTi would be 86-92 kG.)

Figure 13 shows the trapping profiles of 60-keV D° and T° beams which are injected in the plasma midplane. The focussed beam diameter is 30 cm, and the beam axis is tangent to a radius 20 cm inside the magnetic axis, as shown in Fig. 4(b). While the trapping profiles are quite favorable, if the ion velocity distributions are not ideal (i.e., $\alpha_c > 0$), n_e would have to be increased to maintain the neutron flux (Sect. 3.4). Acceptable trapping profiles are still obtained for $\bar{n}_e$ up to 5×10^{13} cm^{-3}, so that if $\alpha_c = 1$ ($\langle\sigma v\rangle$ reduced by 62%), the neutron flux is reduced by 37%. (At the same time, the injected power must be increased to about 30 MW.)

In this device about 5.5 MW of fusion alpha particles are generated, of which approximately 50% are confined in the plasma. While some of the remainder will be swept out by the divertor, most nonconfined alphas will have orbits that carry them to the first wall.

4.3 Burn Cycle

The sequence of events during a burn cycle is the following:

(1) Form target plasma and ramp up current:	2 s
(2) Begin injection and attain equilibrium plasma:	1 s
(3) Burn period (continuous injection):	$\gtrsim$ 30 s
(4) Shut beams and ramp down current:	1 s
(5) Exhaust vessel to 10^{-6} torr:	10 s

Since all fueling is carried out by the beams, the length of the burn period ($\gtrsim$ 30 s) is detrmined either by impurity buildup, or by the volt-sec available in the transformer core to drive the toroidal current. In the present design, $I_p = 1.4$ MA can be maintained for 32 s with a maximum field in the core of 60 kG. A 30 s burn period results in a duty factor of 68%. Since plasma current can also be driven by the beams under many conditions [13], significantly longer burn periods and duty factors seem possible. In practice, impurity buildup may eventually cause a drastic reduction in neutron flux, necessitating shutdown and exhaust. While 5-10% of the injected energy is lost in the form of charge-exchange neutrals, the wall sputtering problem in the CIT should still be much less severe than in more conventional tokamak operation, since most of the injected energy goes out via electron transport and radiation (i.e., $\tau_E \ll \tau_h$). At any rate, impurity buildup should be limited by the poloidal magnetic divertor installed to minimize recycling (Sect. 2.4).

4.4 Neutron Source Characteristics

Table II lists the characteristics of the CIT neutron source for the plasma conditions of Table I. The uncollided flux during the burn is 8.4×10^{12} n/cm^2/s, so that an annual fluence of 10^{20} n/cm^2 requires a plant factor of 38%. For a minimum duty factor of 68% (Sect. 4.3), the down time can be as large as 44%. Accessibility considerations limit the wall area useful for testing purposes to the outer torus region, where the total area is about 65 m^2. Considerable space in this latter region is taken up by beam injection ducts (~2 m^2), diagnostic ports (~3 m^2), bellows sections (~8 m^2), protection plates opposite beam injection ducts (~6 m^2), and miscellaneous vacuum structures (~5 m^2.) Nevertheless, the area available for test samples is at least 30 m^2, so that about 25% of the total neutron output of 10^{19} n/s can be utilized. (In addition, materials left untouched on the inner torus wall for the lifetime of the machine would be subjected to a total fluence ~ 10^{21} n/cm^2, and might exhibit significant bulk-radiation damage.)

5. SOME ENGINEERING ASPECTS OF THE CIT REFERENCE DESIGN

5.1 Neutral Beam Injectors

The characteristics of the neutral beam injection systems are given in Table III. For equal densitites of D^+ and T^+ in the plasma, the T° injection rate need be only 2/3 as large as the D° injection rate, since the triton slowing-down time is about 1.5 times the deuteron slowing-down time. The total beam-duct aperture is specified for 6 beam lines. The use of a larger number of beam lines would result in intolerable crowding of injector assemblies outside the tokamak, while the total area of the beam ducts would have to be increased, in order to ensure penetration [19]. (Note that all vacuum pumping is carried out via the beam ducts and the divertor channels.) The specified injector efficiency of 60% compares with values of 50-60% that have been achieved with beam injectors at ORNL and Berkeley operating at 40 keV and 20 keV, respectively. This efficiency should be maintained at 60 keV energy [20], even without the use of direct conversion. However, a serious drawback of present injector systems is that the ion beams contain 20-30% molecular ion content, so that the efficiency of production, at the plasma, of 60-keV D^+ and T^+ woulld be somewhat less that 60%, unless the D_2^+ and D_3^+ components are separated out before acceleration [20], or the source composition is improved. While present 40-keV injectors with water-cooled grids have been operated for pulse lengths of only 0.3-0.5 s [21], the pulse limitation is due to power supplies and pumping load; there appears to be no insuperable obstacle to steady-state high-power operation.

Table IV shows the tritium throughput characteristics of the CIT facility. The throughput of 12 g/hr is sufficiently large that on-line reprocessing is mandatory. The total inventory specified is rather small, but requires a turn-around time (beam injection, collection, purification, re-injection) of 1.5 day or less. The annual consumption of 760 g represents an operating cost of approximately $3M.

5.2 Power Requirements

Table V shows the power requirements of the CIT electrical systems. The copper windings of the hybrid TF magnet (Fig. 12) dissipate 20 MW, while providing a field of 10 kG on the magnetic axis. These coils are operated steady state, in order to avoid setting up eddy currents in the NbTi windings. The large peak power in the OH circuit is due to the inductive load during the 1-s discharge current ramp-up at the beginning of each burn cycle, before beam injector turn-on. The EF power requirement, which includes the divertor-field coils, remains large after the beam injectors are turned on, as the equilibrium pressure distribution in the plasma is being established. The OH and EF coils are water-cooled copper. Although the OH and EF resistive power losses could be essentially eliminated by going to superconducting windings, the requisite technology is probably too ambitious for a near-term machine.

During the off-period of the burn cycle ($\lesssim$ 30%), the total power requirement drops to about 35 MW, so that 65 MW must be switched approximately once per minute. This requirement is sufficiently lenient that it is feasible to supply all the facility power (97 MW) directly from a utility grid via transformer-rectifier systems.

5.3 Utilization of the Test Volume

The present design provides a semi-toroidal shell of 20-cm thickness for installation of test samples (Fig. 12). To enhance accessibility, the shielding material around the outer torus may have to be removable. An increase in thickness would make the test region more versatile, and minimize down-time. Since the magnetic field is relatively small on the large major-radius side, this increase can be obtained at modest cost by specifying a larger TF coil bore. The additional space could be used to increase the effective neutron flux at the test samples by optimizing backscatter. For example, a high-Z scatterer such as lead or steel could be placed behind the test samples, in order to minimize energy degradation of backscattered neutrons. Neutron multiplication in a Be reflector, backed by graphite, would lead to a large increase in flux at the test sample. It is important to note that large increases in effective neutron yield by backscattered energetic neutrons would be difficult to achieve in small-volume neutron sources, but are relatively straightforward to attain in the present facility because of the enormous illuminated area.

A test volume 20-40 cm thick could also be used to investigate heat transfer in small blanket modules, although the thermal load in the CIT is relatively small (20 W/cm^2 peak neutron power). Cross sections for neutron multiplication, breeding, activation, and gas production could of course be readily determined.

5.4 Facility Cost

The estimated costs of the various subsystems of the CIT radiation facility are given in Table VI. The cost of the neutral beam injectors, including power conversion equipment, is taken as \$600/kW. The power equipment for the various magnetic coils consists largely of the transformer-rectifier systems required for coupling to the utility grid. The time-averaged

thermal power generated in the facility is 80-85 MW; the cost of a cooling tower has not been included. Clearly, the total cost could be substantially reduced by making use of existing building facilities with remote handling equipment and hot cells.

For a 50% plant factor, the total cost of $139M gives a "specific-cost neutron yield" of 3.4×10^{16} n/s/M$. While only 25% of the 14-Mev neutron output is directly utilized, a similar fraction applies to other proposed radiation test facilities [1,2]. The neutron yield referenced to power consumption is 10^{17} n/s/MW. If we measure cost-effectiveness by either of these quantities, the CIT is many times more favorable than other proposed radiation sources for uncollided flux levels ~ 10^{13} n/cm^2/s.

5.5 Required Technological Development

The size of the CIT plasma is similar to that of tokamaks presently coming on-line, and the required beam injector performance has already been approached. Nevertheless, considerable development of plasma and reactor technologies is required for successful construction and reliable operation of the CIT facility. These development needs are briefly outlined in the following.

Neutral Beams. As discussed in Sect. 5.1, the principal advances required in neutral-beam technology are post-acceleration of high current ion beams to 60 keV, reduction of moleclar-ion composition, and cryogenic pumping in the beam ducts to allow steady-state operation. Up to 70 A-equiv. is required per beam line, which can be met by stacking 2 of the 40-A sources now under development [21].

Superconducting Magnet. The NbTi TF coils are D-shaped with bore dimensions 3.2 m x 4.2 m. These coils are sufficiently small that no overwhelming stress problems are expected. The windings, stabilization, and structural support for such coils are essentially state-of-the-art.

Plasma Divertor. The PDX tokamak presently under construction will be equipped with a poloidal magnetic divertor whose configuration can be readily changed [22]. The PDX plasma dimensions (a_p = 42 cm, A = 3.3, $K \leq 1.5$) are fairly similar to those in the present design, and 4 MW of neutral beam injection at 40 keV will be provided. This beam injection, together with divertor operation to prevent recycling and control impurities, will enable thorough testing of CIT plasma operation, especially minimization of the cold-ion population. Thus the PDX device is a "critical assembly" for the CIT radiation facility.

Remote Handling. The special equipment needed for remote maintenance and disassembly of highly activated tokamak reactor components has not been developed to any extent. While a great deal of relevant design has been carried out recently in conjunction with the proposed TFTR, JET, and T-20 devices, work in this area would have to be substantially accelerated in order that remote handling of a near-term device be feasible.

Tritium. The handling and containment of tritium (which has not yet formed part of any controlled fusion program) is perhaps the area that presents the most severe technological problems. The CIT tritium throughput

of 12 g/hr requires a closed-cycle chemical processing plant, including gas purification, absorption on solid material, regeneration, and delivery. The operation of neutral-beam injectors with tritium, and the control of tritium diffusion through various machine components, are problems not yet resolved.

All these technologies must be pursued, in any event, in the course of developing tokamak power reactors. It is this technological relevance, combined with enormous test area, true fusion neutron spectrum as well as the energetic particle and photon bombardment characteristic of tokamak devices, that make the CIT a cost-effective surface radiation test facility.

ACKNOWLEDGMENT

This work was supported by the United States Energy Research and Development Administration Contract E(11-1)-3073.

REFERENCES

1. P. J. PERSIANI, "Neutron Source Considerations for the CTR Materials Program," Rep. AP/CTR/TM-2, Argonne National Laboratory, (1972).

2. P. J. PERSIANI, "Study of the Development of Neutron and Plasma Radiation Test Facilities for the CTR Materials Program," *Proc. First ANS Topical Meeting on the Technology of Controlled Nuclear Fusion*, San Diego, (1974), Vol. 1, p. 283.

3. D. L. JASSBY, R. M. KULSRUD, *Bull. Am. Phys. Soc.* 20, 658 (1975); R. M. KULSRUD, D. L. JASSBY, "Neutralized Colliding-Beam Toroidal Fusion Reactors," USERDA Rep.MATT-1114, Princeton Plasma Physics Laboratory, (1975); D. L. JASSBY, R. M. KULSRUD, Y. C. SUN, "Colliding-Beam Tokamak Plasmas," *Proc. 7th European Conference on Controlled Fusion and Plasma Physics*, Lausanne, (1975), to be published.

4. D. L. JASSBY, "Reactor Aspects of Counterstreaming-Ion Tokamak Plasmas," USERDA Rep. MATT-1145, Princeton Plasma Physics Laboratory, (1975).

5. R. M. KULSRUD, Y. C. SUN, D. L. JASSBY, unpublished.

6. F. W. PERKINS, "Ion-Streaming Instabilities: Electromagnetic and Electrostatic," USERDA Rep. MATT-1141, Princeton Plasma Physics Laboratory, (1975).

7. K. BOL, et al, *Proc. 5th International Conference on Plasma Physics and Controlled Nuclear Fusion Research*, Tokyo, (1974), Paper CN-33/A4-1 (to be published); L. A. BERRY, et al, ibid., Paper CN-33/A5-2; J. G. CORDEY, et al, *Nucl. Fusion* 15, 441 (1975).

8. R. R. PARKER, B. COPPI, Massachusetts Institute of Technology, private communication.

9. P. E. STOTT, et al, *Nucl. Fusion* 15, 431 (1975).

10. H. L. BERK, et al, "Microinstability Theory of Two-Energy-Component Toroidal Systems'" USERDA Rep. MATT-1127, Princeton Plasma Physics Laboratory, (1975), App. C.

11. T. E. STRINGER, *Nucl. Fusion* 12, 689 (1972).

12. J. P. GIRARD, D. MARTY, P. MORIETTE, *Proc. 5th International Conference on Plasma Physics and Controlled Nuclear Fusion Research*, Tokyo (1974), Paper CN-33/A17-2 (to be published).

13. D. L. JASSBY, unpublished.

14. T. OHKAWA, *Nucl. Fusion* 10, 185 (1970).

15. R. W. CONN, D. L. JASSBY, "A Tokamak Engineering Test Reactor," Univ. of Wisconsin Rep.FDM-119 (1975), and these proceedings.

16. J. G. CORDEY, W. G. F. CORE, to be published.

17. P. J. REARDON, Princeton Plasma Physics Laboratory, private communication.

18. D. M. MEADE, et al, *Proc. 5th International Conference on Plasma Physics and Controlled Nuclear Fusion Research*, Tokyo (1974), Paper CN-33/A15-4 (to be published).

19. A. C. RIVIERE and J. SHEFFIELD, "Transfer Efficiency of Intense Neutral Beams," *Nucl. Fusion* (submitted for publication).

20. J. H. FINK, "Power Efficiencies of Neutral Beam Systems" Rep. UCRL-51650, Lawrence Livermore Laboratory (1974).

21. L. D. STEWART, et al, "Extraction System Design for a 50-A, 50-keV, 2-sec Ion Beam," *Proc. 2nd Symposium on Ion Sources and Formation of Ion Beams*, Berkeley, (1974), Paper II-8.

22. *Proceedings of the 6th Symposium on Engineering Problems of Fusion Research*, San Diego (1975), (to be published).

TABLE I

Plasma Parameters of the CIT Radiation Facility

R_o	2.8 m
a_p	0.55 m
Aspect ratio	5.1
Elongation (D-shape)	1.3
K = circum. / $2\pi a_p$	1.40
Midplane wall radius	0.75 m
Wall area	115 m^2
B_t on magnetic axis	40 kG
Maximum B_t at NbTi coil	65 - 70 kG
I_p	1.4 MA
q at limiter	3.0
$\bar{n}_e$	3.9×10^{13} cm^{-3}
$\bar{T}_e$	4.0 keV
$\bar{n}_e \tau_E$	2.1×10^{12} $cm^{-3}s$
Beam energy	60 keV
λ_t / a_p	0.91
$\bar{n}_i \tau_h$	1.8×10^{13} $cm^{-3}s$
β_p	3.4
Q (ideal)	1.32
P_f	1.06 W/cm^3
Injection power	21 MW
Total neutron power	22 MW
Total thermal power	49 MW

TABLE II

CIT Neutron Source Characteristics

Neutron intensity[a]	9.6×10^{18} n/s
Neutron power	22 MW
Neutron wall loading	0.19 MW/m^2
Neutron flux	8.4×10^{12} $n/cm^2/s$
Pulse length	$\geq$ 30 s
Annual fluence at 50% plant factor	1.3×10^{20} n/cm^2
Wall area available for test samples	30 m^2

[a]All numbers refer to uncollided 14-MeV neutrons.

TABLE III

Neutral Beam Injection Systems

Injection energy	60 keV
Injection power	12.6 MW D° 8.4 MW T°
Injection current	210 A(equiv.) D° 140 A(equiv.) T°
Number of beam lines	6
Total beam aperture	1.75 m^2 at 0.02 A/cm^2
Fraction of wall area	1.5%
Overall efficiency	60%
Power consumption	35 MW(e)

TABLE IV

Tritium Throughput

Throughput at 75% duty factor	12 g/hr
Throughput at 50% plant factor	69 kg/yr
Fractional burn-up per pass	1.1 %
Annual consumption at 50% plant factor	760 g/yr
Total inventory	500 g
Reprocess time	1.5 da

TABLE V

Power Consumption

Hybrid magnet	20 MW
Beam injectors[a]	35 MW
OH coils (current start-up only)	26 MW peak
OH coils (resistive)	9 MW
EF coils	21 MW peak
Miscellaneous plant	12 MW
Total CIT facility[a]	97 MW

[a]Beam injectors are not operated during current start-up.

TABLE VI

Estimated Cost of CIT Radiation Test Facility

Tokamak Components	Cost (M$)[a]
TF coils	14
Refrigeration	4
Structural support	2
OH, EF coils	4
Neutral beam injectors	13
Vacuum vessel and equipment	6
Tritium handling system, incl. inventory	9
Shielding	6
	58
Auxiliary Systems	
Electrical conversion equipment for TF, OH, EF coils	12
Remote maintenance	10
Heat removal	4
Instrumentation and controls	6
Essential plasma diagnostics	1
	33
Miscellaneous Plant	
Buildings, incl. hot cell	18
Misc. plant equipment (energy distrib., air cond.)	7
	25
Engineering and administration @ 20%.	23
TOTAL	$139M

[a] 1975 Dollars

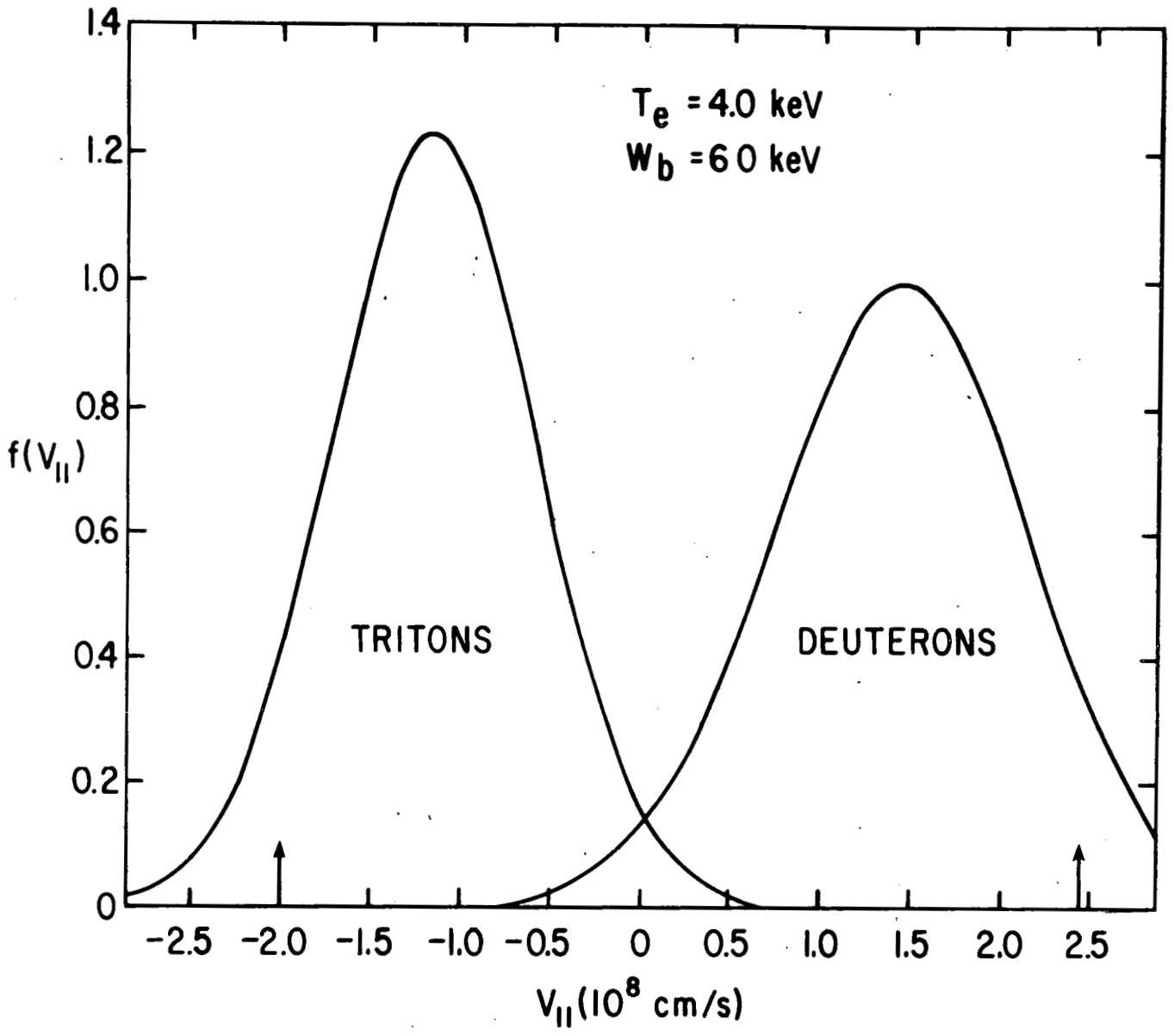

753517

Fig. 1. Counterstreaming-ion velocity distributions parallel to the toroidal magnetic field. Injection velocities are indicated by the arrows. The two distributions have the same density and total energy

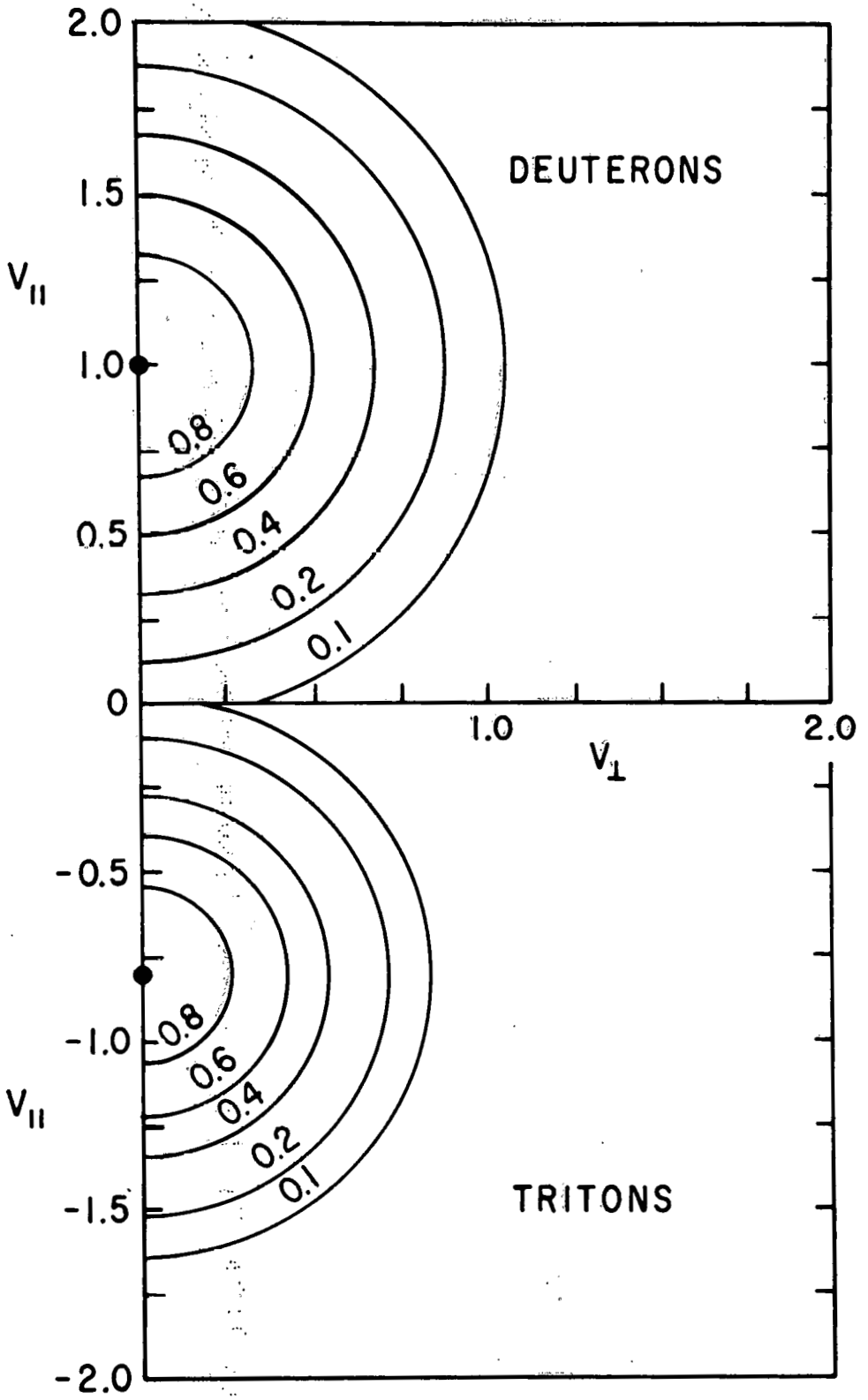

Fig. 2. Contours of displaced-Maxwellian velocity distributions of counterstreaming D and T ions, for steady-state injection at 60 keV, and T_e = 4.0 keV. Velocities are normalized to 1.46×10^8 cm/sec. The large dots indicate f(v) = 1.0.

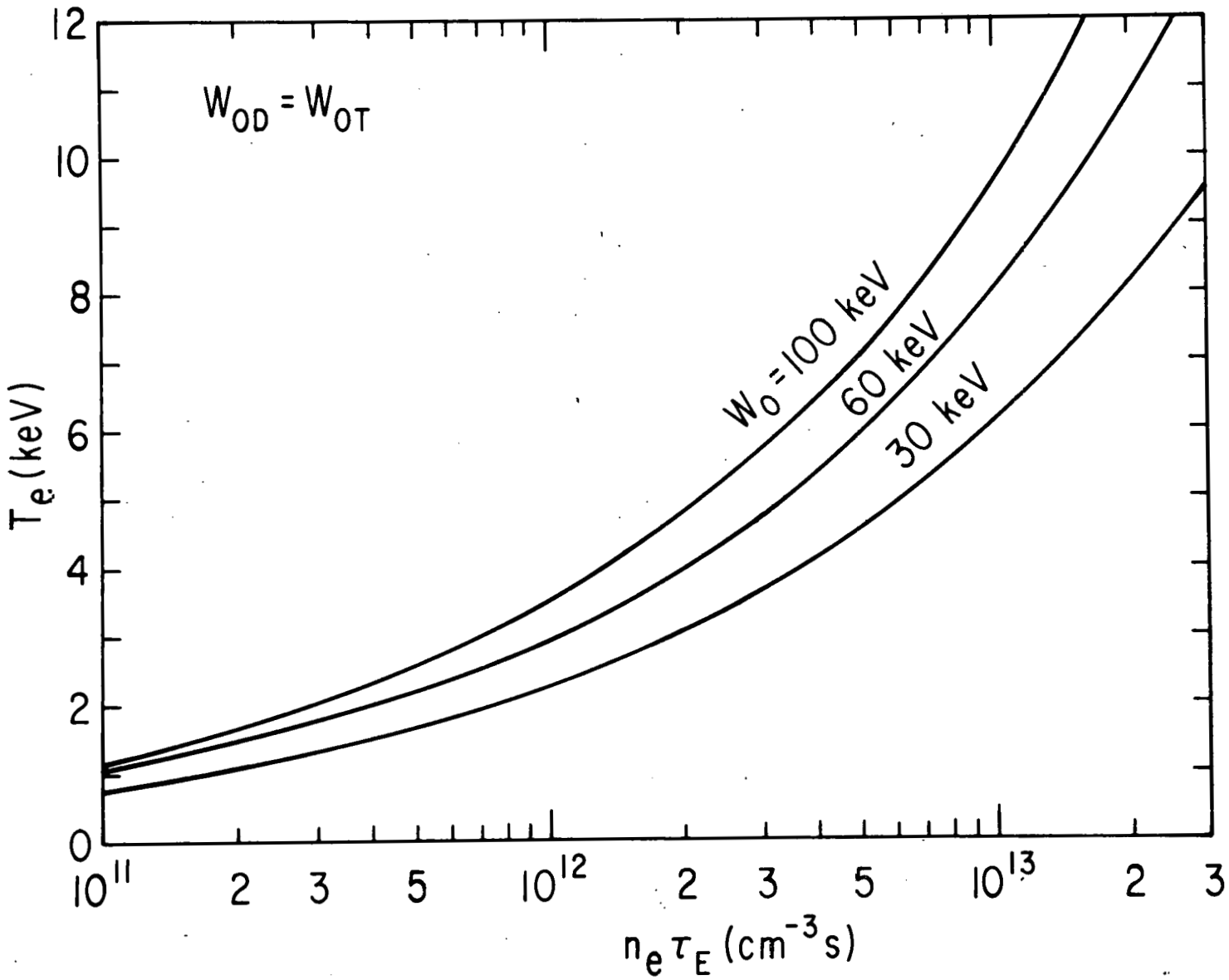

753765

Fig. 3. Dependence of T_e on electron energy confinement time for various injection energies. Steady-state CIT operation.

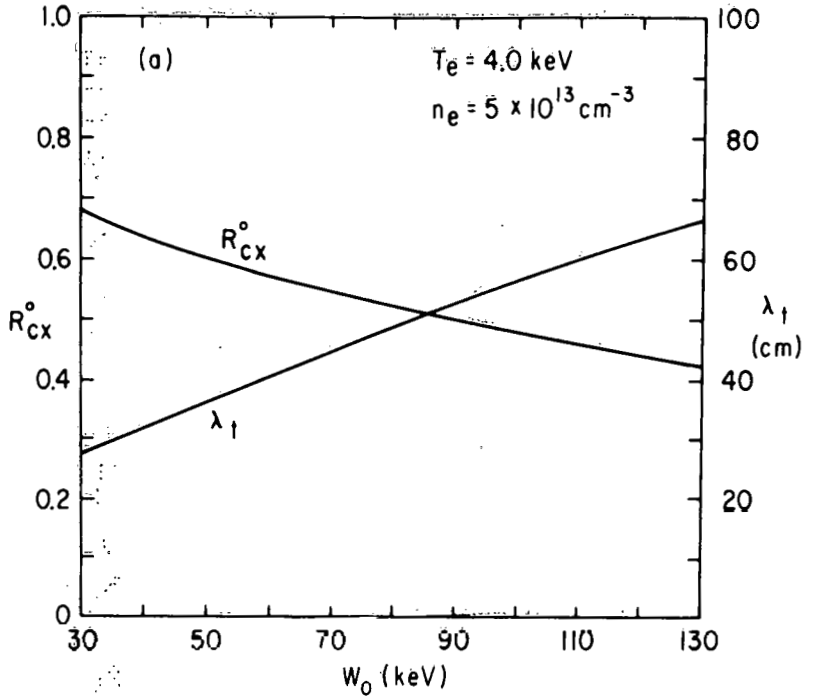

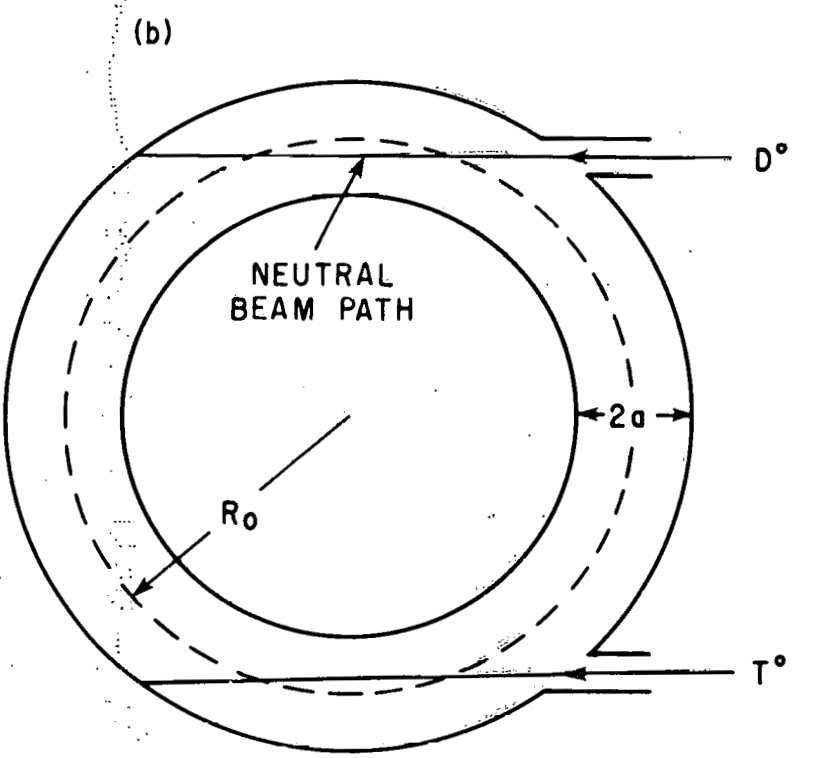

753709

Fig. 4. (a) Trapping length λ_t of deuterium atoms of energy W_o injected into a counterstreaming-ion plasma formed by injection at W_o. R^o_{cx} is the fraction of atoms trapped by charge exchange. (b) Geometry of tangential neutral-beam injection into a torus.

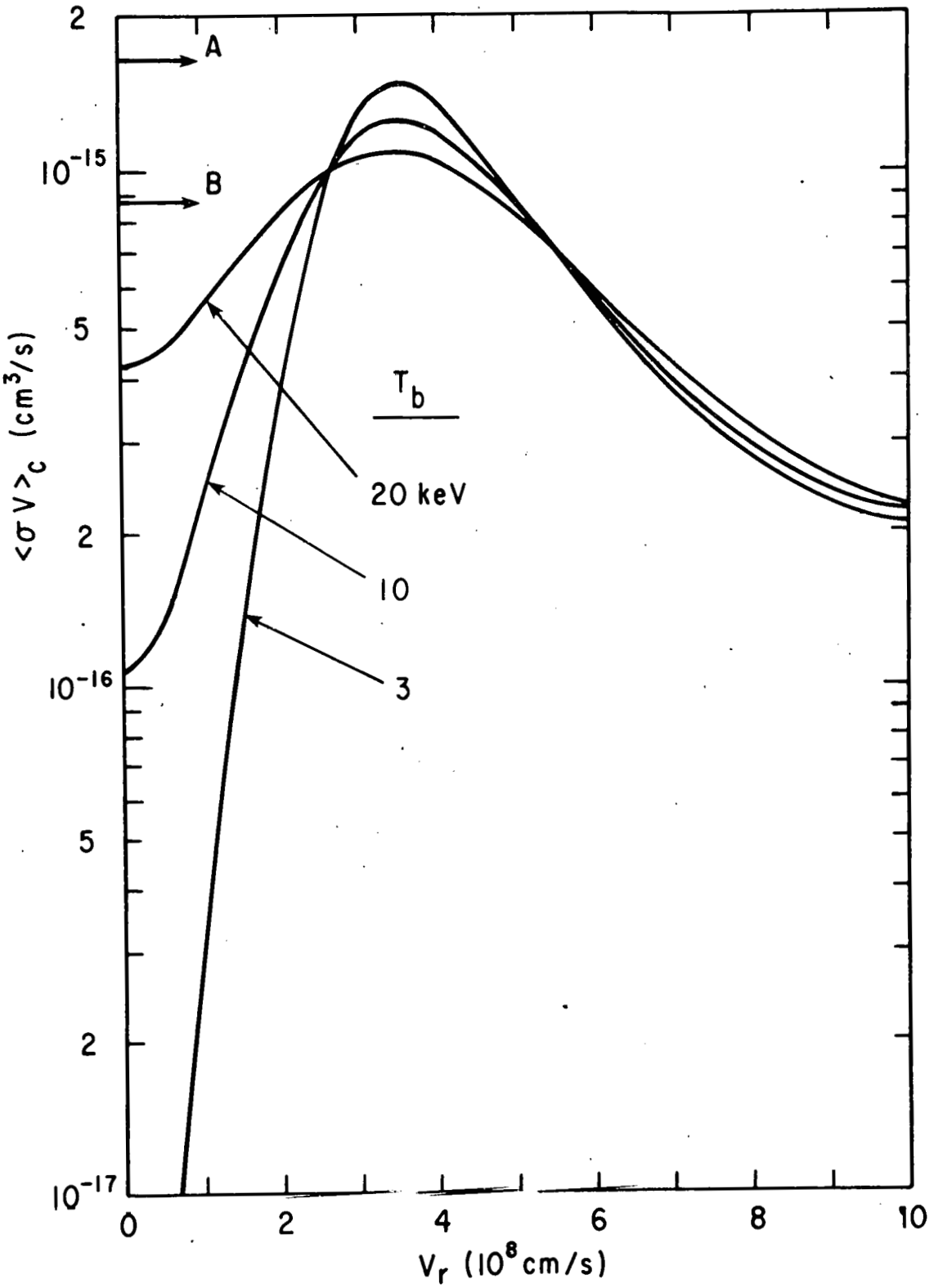

Fig. 5. Fusion reactivity of D and T displaced-Maxwellian distributions, each of temperature T_b, with relative displacement velocity v_r. The maximum reactivity of a D-T beam-target system is denoted by A. The maximum reactivity of a thermonuclear D-T plasma is denoted by B.

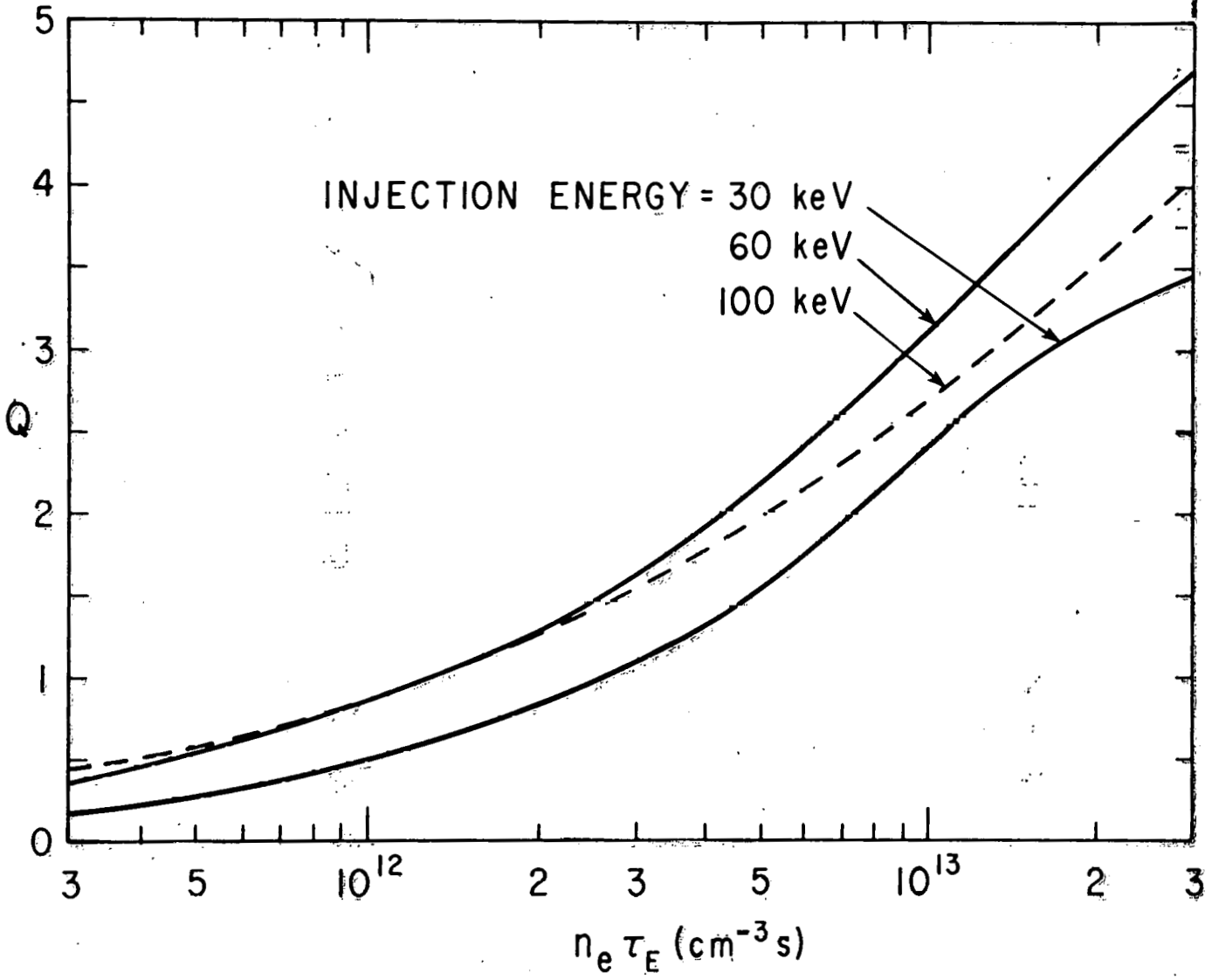

753710

Fig. 6. Dependence of fusion power amplification Q on electron energy confinement time for various injection energies. Steady-state CIT operation, with $W_{oD} = W_{oT}$. 17.6 MeV per reaction.

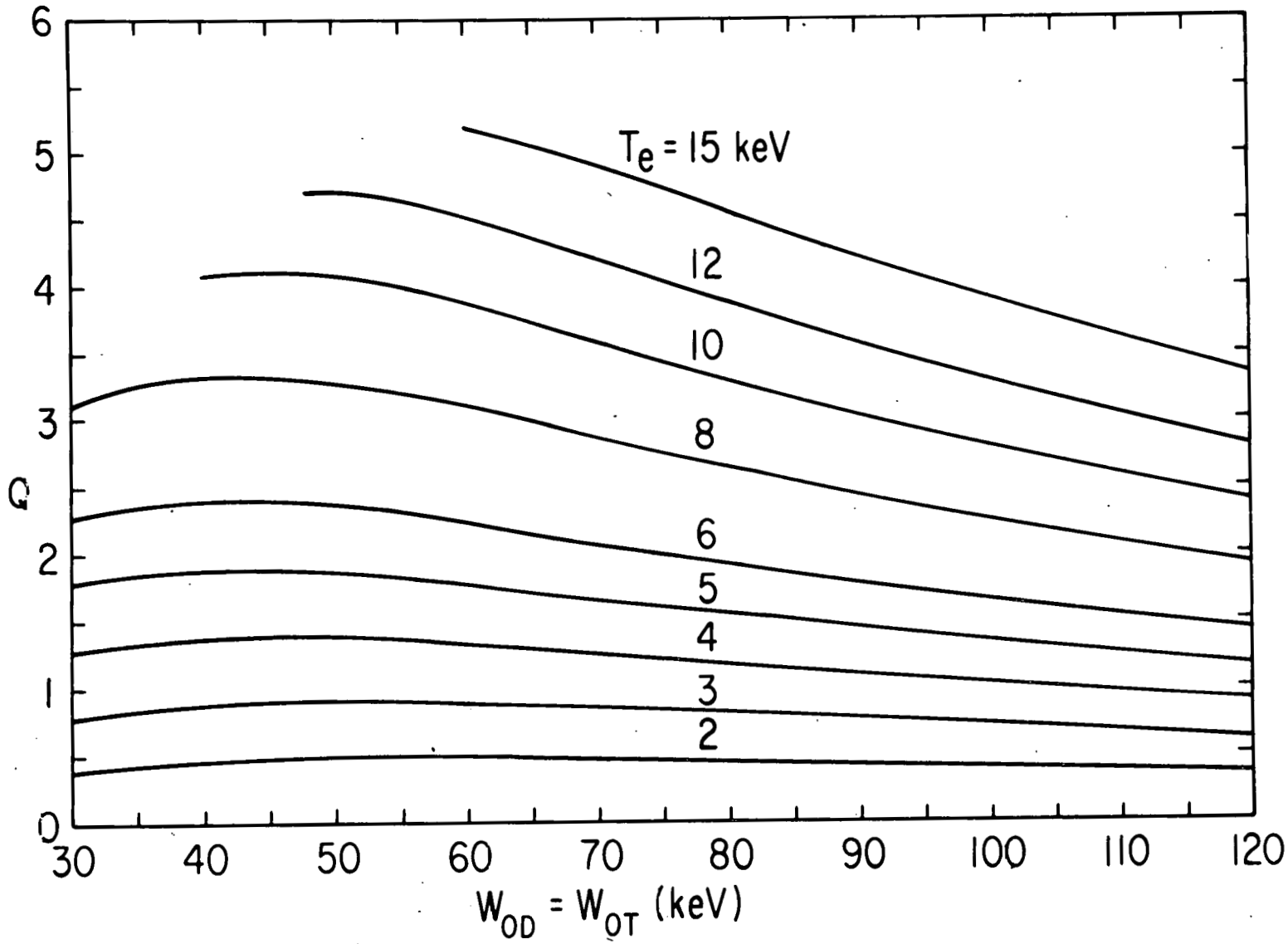

753456

Fig. 7. Fusion power amplification Q for steady-state counterstreaming-ion operation in D-T, as a function of injection energy and T_e. 17.6 MeV per reaction.

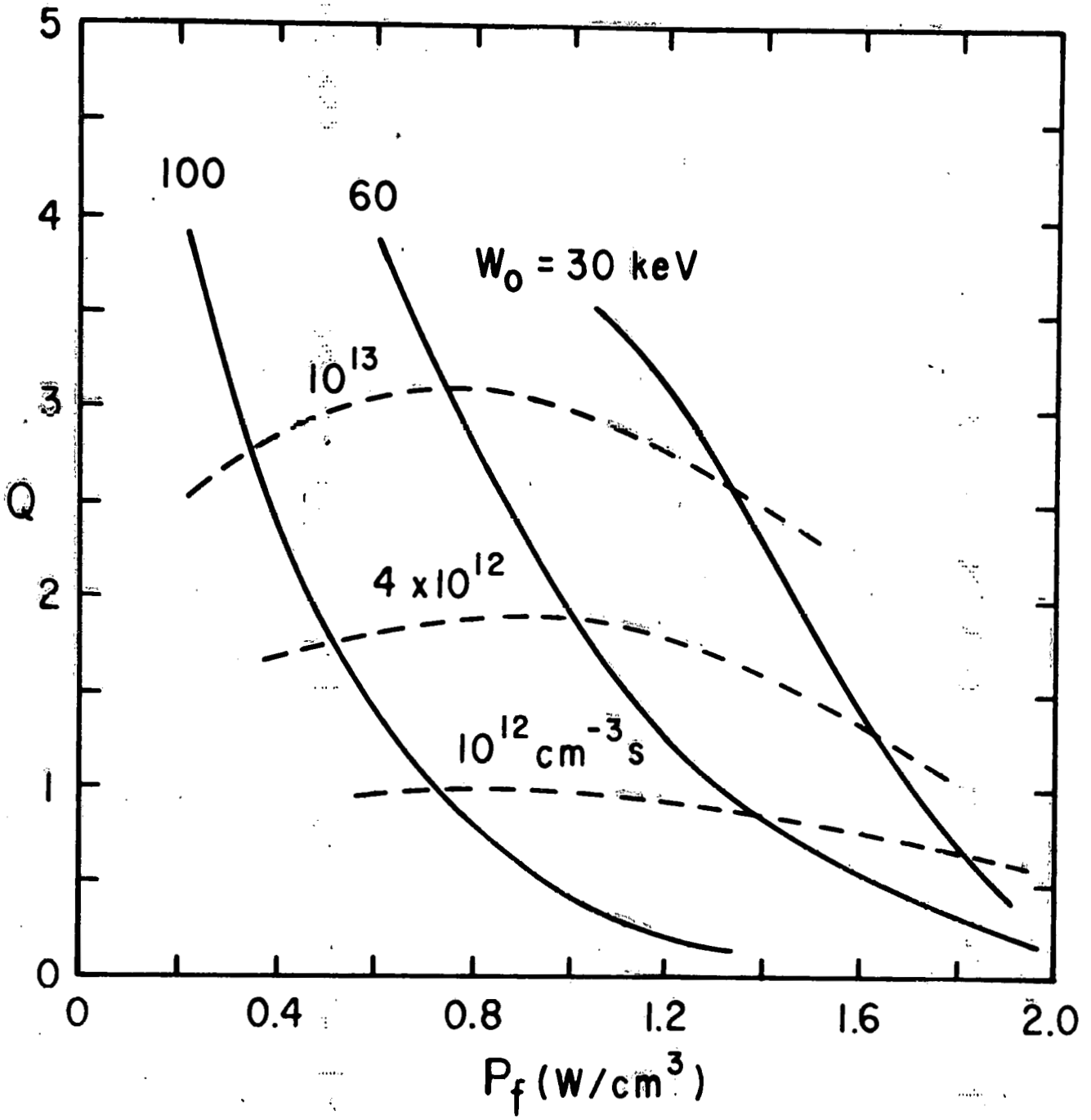

753459

Fig. 8. Fusion power amplification Q versus power density P_f for a counterstreaming-ion D-T plasma. The solid curves are contours of constant injection energy, and the dashed curves are contours of constant $n_e \tau_E$. B_t = 50 kG, A = 5.0, q = 2.5, β_p = 3.0.

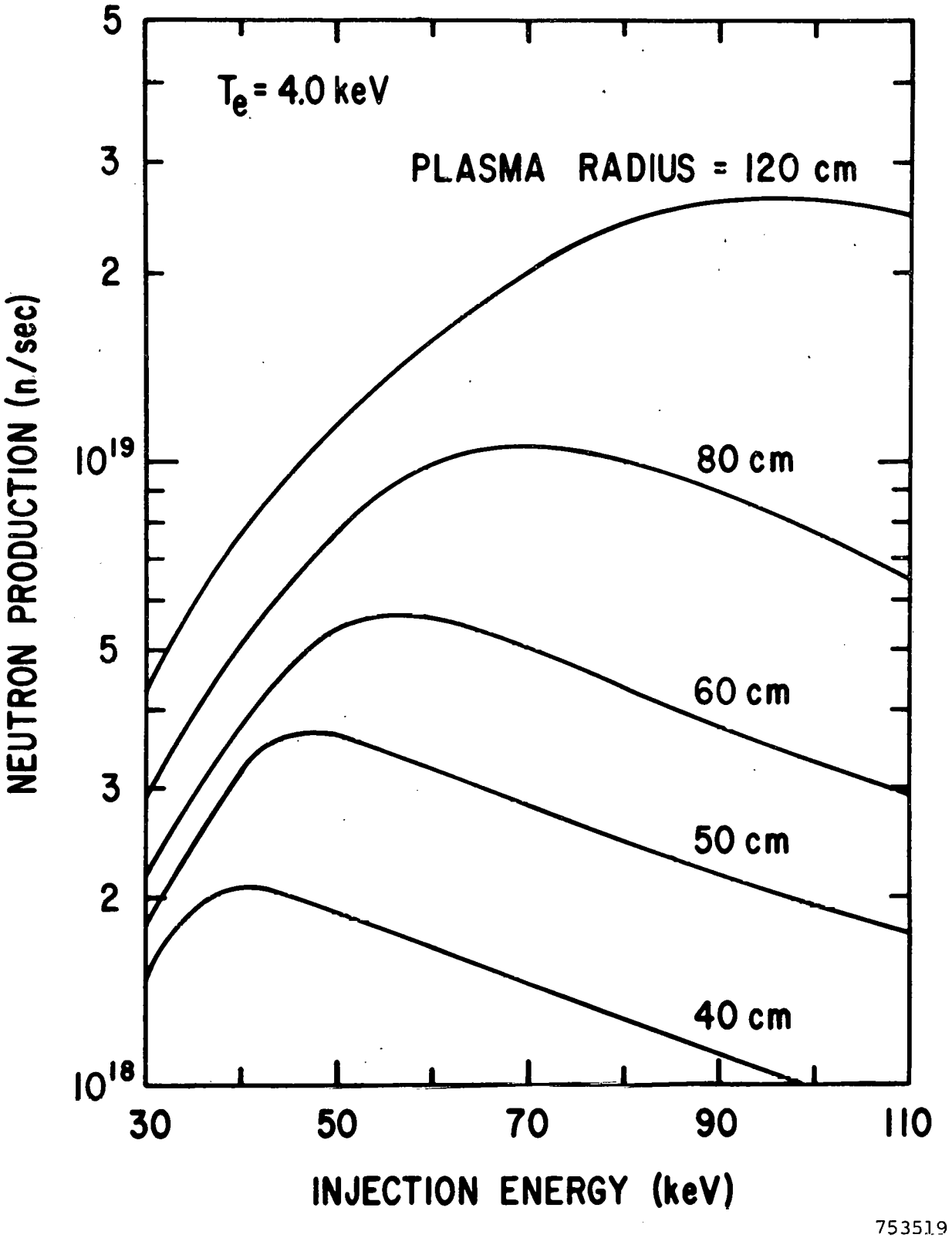

Fig. 9. Production rate of 14-MeV neutrons from D-T counterstreaming-ion tokamak plasmas of circular cross section. Deuterons and tritons are injected with the same energy. B_t = 40 kG, A = 5.0, q = 2.5, $\beta_p \lesssim 3.3$, $\lambda_t \gtrsim a_p$.

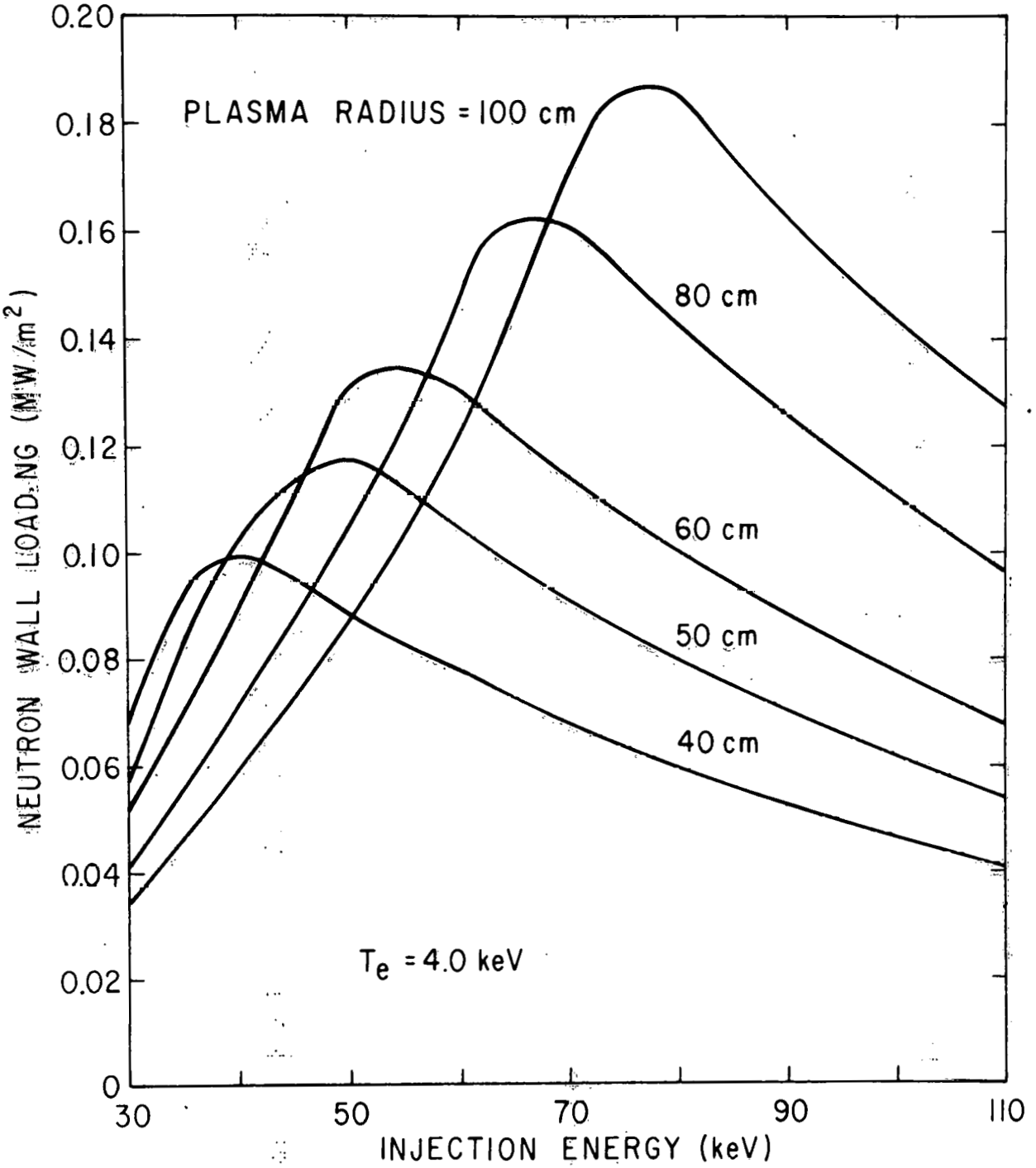

Fig. 10. Neutron wall loadings (uncollided 14-MeV) in D-T counterstreaming-ion tokamak plasmas of circular cross section. Deuterons and tritons are injected with the same energy. B_t = 40 kG, a = 5.0, q = 2.5, $\beta_p \lesssim 3.3$, $\lambda_t \gtrsim a_p$.

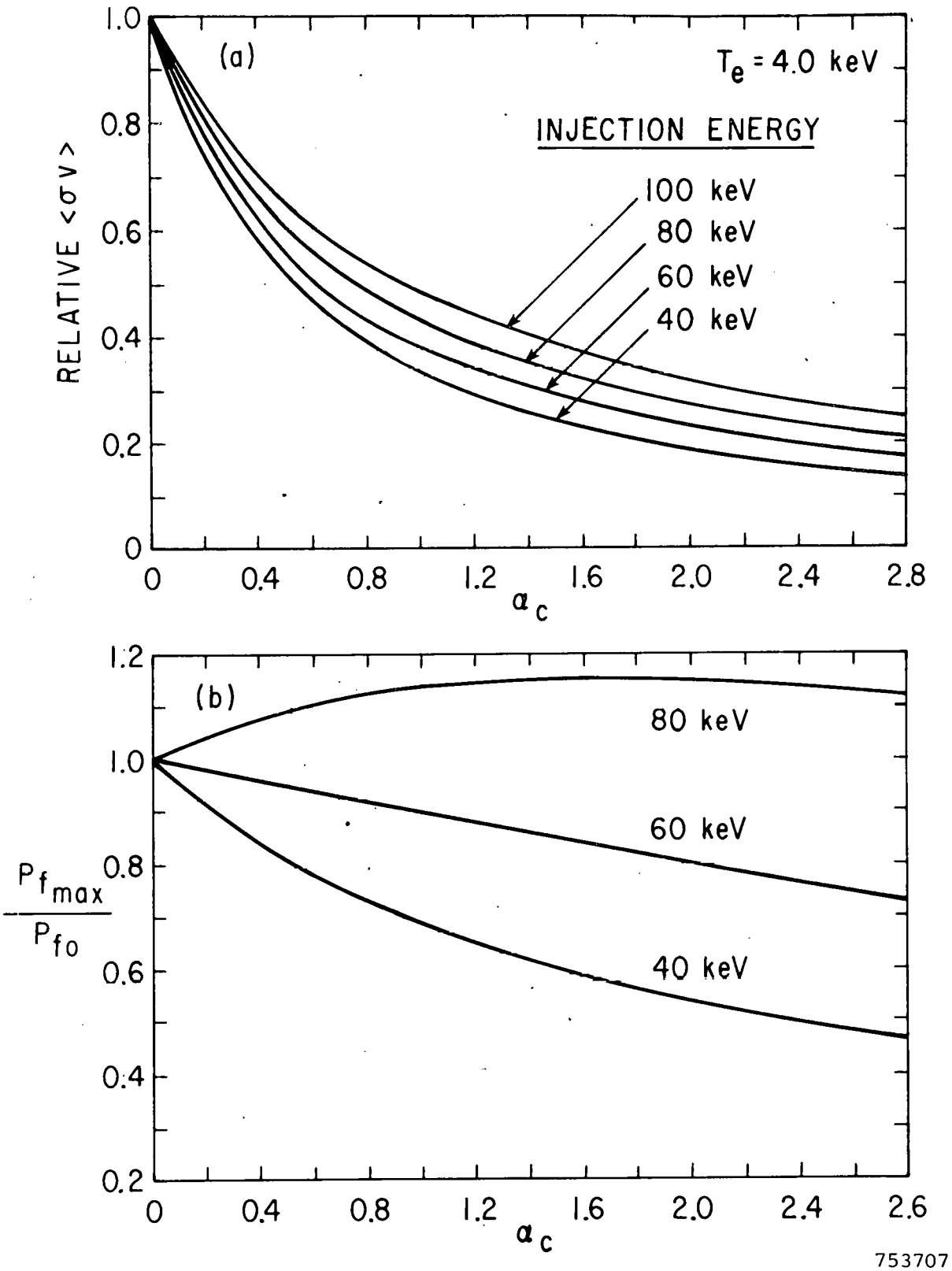

Fig. 11. (a) Reduction in CIT fusion reactivity <σv> by a Maxwellian "cold-ion" population at temperature T_e. α_c (cold-ion density)/(energetic-ion density). (b) Maximum fusion power density in a CIT plasma with a Maxwellian "cold-ion" population at 4.0 keV. The plasma density is increased with α_c so that the total plasma pressure is constant.

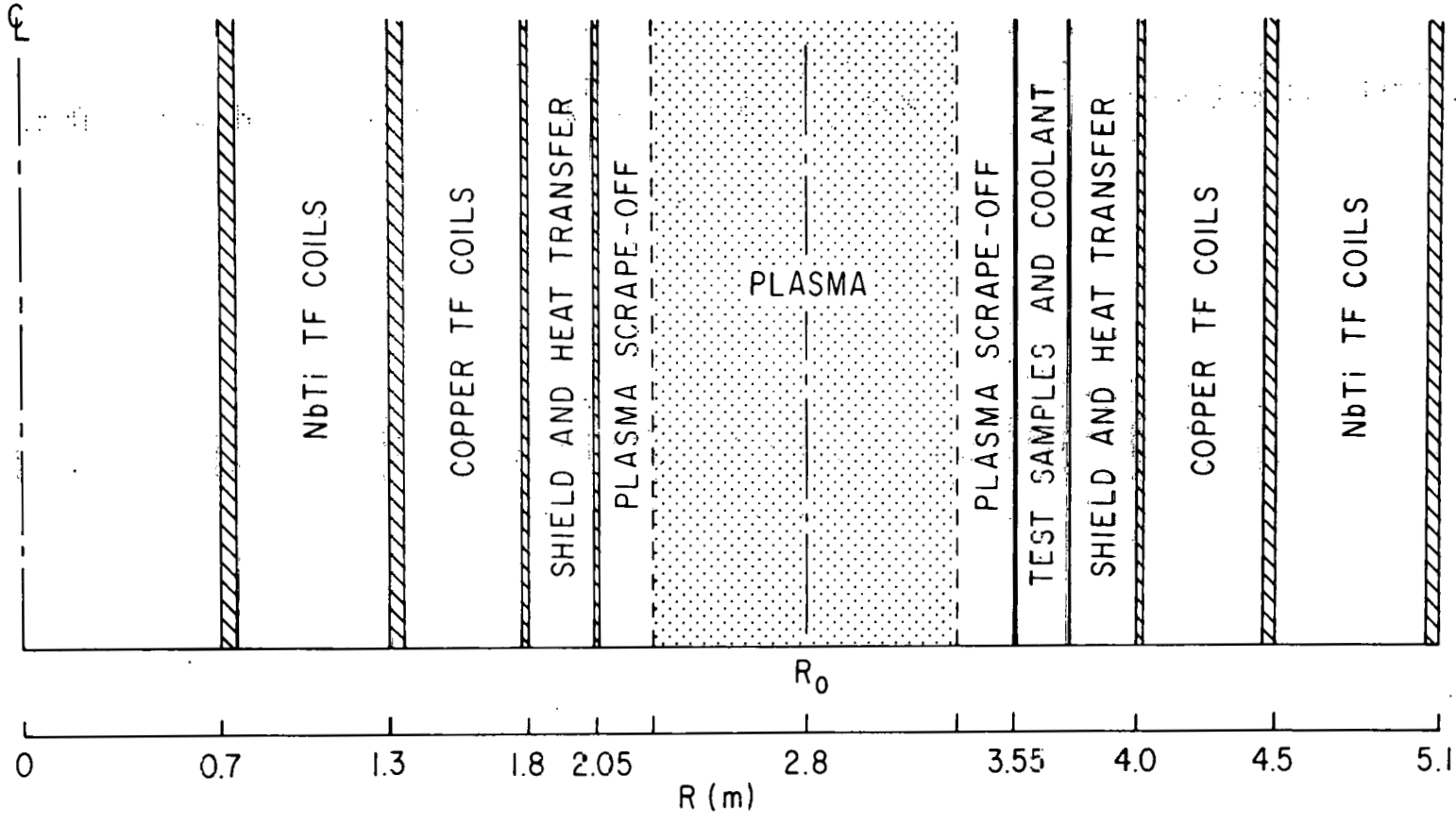

753706

Fig. 12. Schematic layout of the CIT radiation facility. The test-sample volume is a 20-cm shell on the outer region of the torus. The toroidal field on the magnetic axis is 40 kG.

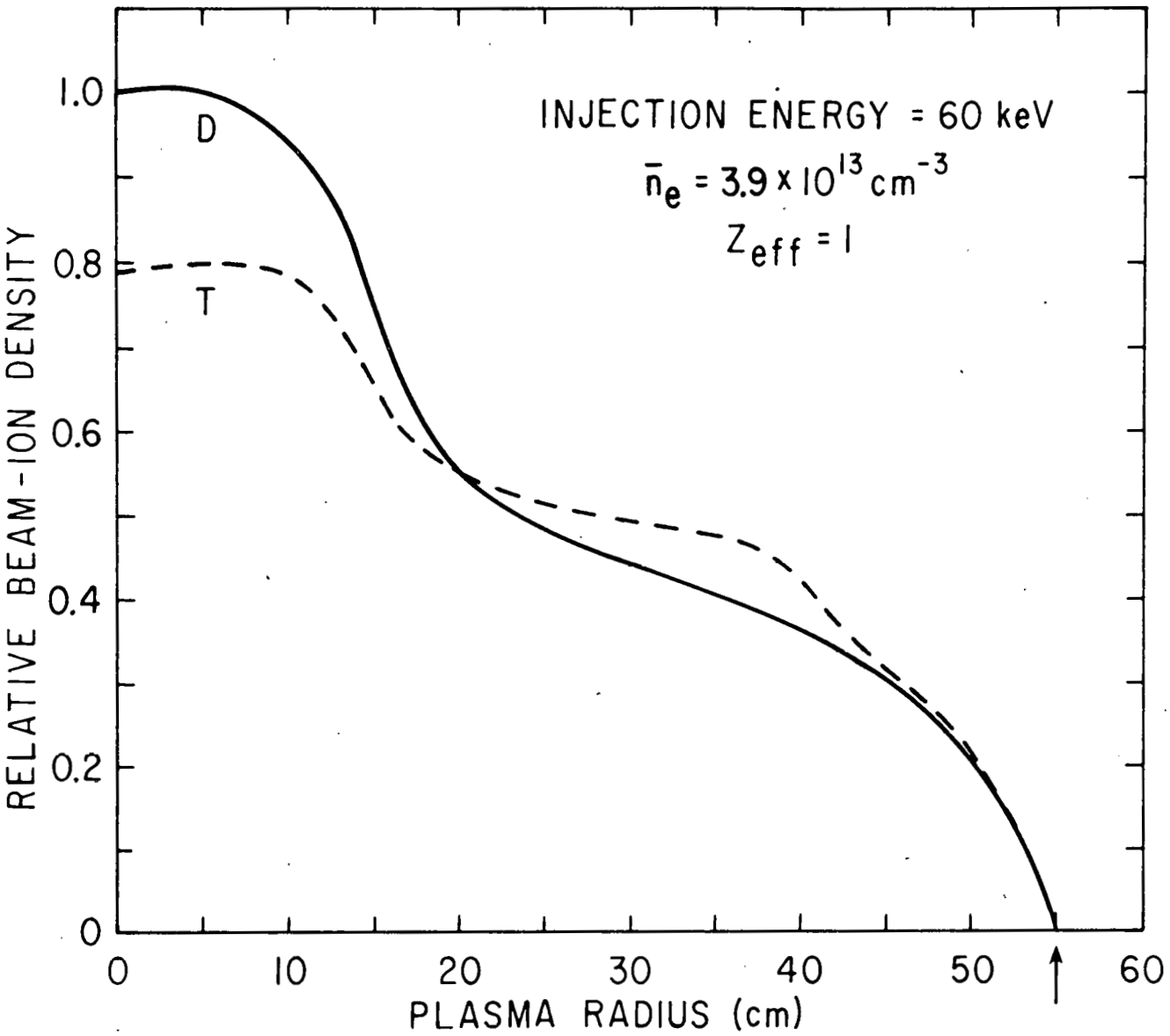

753708

Fig. 13. Trapping profiles of 60-keV D and T neutral beams injected tangentially into the CIT plasma, as shown in Fig. 4 (b). The arrow indicates the edge of the current channel.

***